Applied Catalysis B: Environmental 336 (2023) 122924

Contents lists available at ScienceDirect

Applied Catalysis B: Environmental

journal homepage: www.elsevier.com/locate/apcatb

Nanographite: A highly active and durable metal-free ozonation catalyst with application in natural waters

Antón López-Francés [a], Francisco Bernat-Quesada [b], María Cabrero-Antonino [a], Belén Ferrer [a], Amarajothi Dhakshinammorthy [a,c], Herme G. Baldoví [a,*], Sergio Navalón [a,*]

[a] Departamento de Química, Universitat Politècnica de València, Camino de Vera s/n, Valencia 46022, Spain
[b] Empresa Mixta Valenciana de Aguas SA (EMIVASA), Av. del Regne de València, 28, 46005, Valencia, Spain
[c] School of Chemistry, Madurai Kamaraj University, Madurai 625 021, Tamil Nadu, India

ARTICLE INFO

Keywords:
Heterogeneous catalysis
Metal-free catalysis
Nanographite
Ozonation
Aqueous pollutant degradation
Natural water

ABSTRACT

The development of metal-free heterogeneous catalysts for advanced oxidation processes has emerged as a key focus for both academia and industry. We report on research that seeks to establish a correlation between the crystallographic, physicochemical, textural, and morphological properties of a series of graphite-based solids and their activities as metal-free ozonation catalysts in aqueous media. Our findings show that nanographite (NG) outperforms traditional graphite-based solids, activated carbon and Co_3O_4. The enhanced activity of NG is due to defective nanosized graphitic structures with high surface areas. NG exhibits an exceptional activity, durability, and recyclability that surpasses other known catalysts. Our study employs electron spin resonance and selective quenching experiments that reveal the generation of $^1O_2$ during catalytic ozonation. Significantly, NG shows excellent catalytic efficiency even when using natural surface river water or seawater. This study illustrates the importance of the natural properties of graphite-based materials as active and durable ozonation catalysts in water.

1. Introduction

Advanced oxidation processes (AOPs) are highly preferred among the technologies developed for the degradation of organic contaminants in water, soil, and air [1–10]. These processes involve the generation of reactive oxygen species (ROS) such as $HO^{\cdot}$, $HOO^{\cdot}$ or $SO_4^{\cdot-}$ radicals, as well as $^1O_2$ species. AOPs have attracted considerable interest in industry due to their relatively easy and highly effective implementation and are based on the use of a transition metal-based heterogeneous catalyst together with strong oxidants such as ozone (O_3) [11–13], hydrogen peroxide (H_2O_2) [14,15], peroxymonosulfate (PMS) [10,16,17], and persulfate [17,18], among others [19]. Specifically, catalytic ozonation has been identified as a promising cost-effective AOP for medium and large-scale industrial applications [13,20–25]. Some drinking or industrial water treatment plants already use ozone as an oxidant for efficient treatments. Ozone is a relatively strong oxidant (E^0 =2.05 V, NHE) [26] that can be used for pollutant degradation and water disinfection [25,27,28]. However, under typical conditions, O_3 alone is not sufficiently reactive in water treatments to degrade deactivated aromatic or electron-poor aliphatic pollutants [11]. In contrast, catalytic ozonation has been shown to effectively transform O_3 to ROS that can degrade these types of recalcitrant pollutants [11,12,29]. Oxalic acid is commonly used as an organic model pollutant to evaluate catalyst efficiency under ozonation conditions [29,30]. Oxalic acid in water is almost unreactive towards O_3 under the conditions employed in water treatment [30]. Oxalic acid in water is a byproduct that accumulates during ozonation and is also considered as a refractory organic compound in conventional chemical oxidation [31].

Recently, there has been a growing interest in developing sustainable and efficient metal-free heterogeneous AOP catalysts as an alternative to transition-metal based solids [32–36]. Our group and others have reported on the development of metal-free catalysts such as activated carbon (AC) [37–43], carbon nanotubes (CNTs) [41,44–46], graphite (G) [47,48], graphene-based soilds [47,49], graphitized nanodiamonds [50], and others [26,51–53]. Nanographites (NGs), with their nanometric dimensions and high surface areas, have recently emerged as a promising class of material with potential applications in catalysis [54,55]. Despite the excellent achievements made in the field and the large

* Corresponding authors.
E-mail addresses: hergarba@cam.upv.es (H.G. Baldoví), sernaol@doctor.upv.es (S. Navalón).

https://doi.org/10.1016/j.apcatb.2023.122924
Received 29 September 2022; Received in revised form 21 April 2023; Accepted 26 May 2023
Available online 27 May 2023

number of carbonaceous-based materials, there is a lack of comparative studies on their properties.

G powder (G) is selected as a reference micro-sized material commonly used for catalytic applications including metal-free catalysis [59,60]. Expandable G (EG), a sulfuric acid intercalated flake graphite [61], and their thermal derivatives, *ca* expanded at 600 ºC (EG600), are also graphites traditionally used in catalytic applications [61] and AOP [62,63]. Over the last two decades, interest in using high surface area G (HSAG) for catalytic applications either as a support [64–66] or as a metal-free catalyst [48,67] has been growing and so HSAG is also included for comparison. As far as we know, there is a lack of studies on the use of NG-based materials as metal-free AOP catalysts. This study aims to fill this gap by using NG as metal-free AOP catalyst.

Inspired by these precedents, this study reports on the relationship between the crystallographic, spectroscopy, physicochemical and textural properties of a series of graphite-based solids and their activity as ozonation catalysts for the degradation of oxalic acid in water. Catalyst stability and the reaction mechanisms are also investigated using NG since it shows the highest level of activity among the tested series of materials. Further, the catalytic performance of nanographite is also examined for the degradation of oxalic acid in presence of the inorganic ions or humic acids commonly found in natural waters (including surface river water and seawater).

2. Experimental section

The experimental section includes details of the materials, methods, and procedures employed in this study. The supporting information describes the materials and reagents used, as well as their purities, synthesis of thermally expanded graphites, chemical functionalization of NG, reactivation procedure for the used NG, physicochemical analysis, sampling of natural water analysis, electron paramagnetic resonance (EPR) measurements, and total organic carbon (TOC) analyses.

2.1. Catalytic activity

Catalytic ozonation experiments were conducted as previously reported [50]. The data in this study corresponds to at least three independent experiments and the average values and standard deviations are given. Briefly, a commercially available ozonator was employed to feed ozonized air (150 mg O_3/h; 570 mL/min) using a gas diffuser (pore size 100–160 μm) placed at the bottom of a glass reactor (500 mL). Before starting the catalytic tests, the carbon material (i.e., 100 or 20 mg/L) was dispersed by sonication (450 W, 20 min) in an oxalic acid aqueous solution (i.e., 50, 1000 or 5000 mg/L, 200 mL). The experiments were performed using the following waters: Milli-Q water; surface river water (Turia River, Valencia, Spain), and seawater (Mediterranean Sea, Valencia, Spain). In some experiments, Milli-Q aqueous solutions of NaCl, $NaNO_3$, Na_2SO_4, NaH_2PO_4, and Na_2CO_3 at the corresponding concentrations (i.e., 50, 100, 200 or 5000 mg/L) were also prepared. Humic acid aqueous solutions (i.e., 1, 2, and 5 mg/L) in Milli-Q water were also prepared. The required initial pH was adjusted using 0.1 M NaOH or 0.1 M HNO_3 aqueous solutions. The reaction mixtures containing oxalic acid and the carbocatalyst were then added to the glass reactor. The kinetics of oxalic acid decomposition were measured by analyzing aliquots filtered with 0.2 μm nylon using an HPLC instrument equipled with an UV-Vis detector. The stationary phase of the column consisted of sulfonated polystyrene-divinylbenzene copolymers (ICSep ICE-COREGEL 87H3, 7.8 mm × 300 mm) placed in an HPLC column oven (Echotherm). An aqueous solution of sulfuric acid with 0.001 N was employed as a mobile phase at a flow rate of 0.8 mL/min.

Selective ROS quenching experiments were carried out as described above using a NG sample, but with the addition of 20 mol% of quencher with respect to oxalic acid. Dimethylsulfoxide (DMSO), *t*-butanol, or methanol were used to quench selectively hydroxyl radicals. NaN_3 or furfuryl alcohol were employed as selective $^1O_2$ quenchers, and *p*-benzoquinone was used as a superoxide/hydroperoxide radical scavenger.

The iodometry method was used to monitor the ozone concentration from an ozonator. The ozone concentration at a flow of 570 mL/min was found to be 150 mg/h, while the effective ozone present in the aqueous system was estimated to be 86.8 mg/h. Experimental details of the procedure can be found elsewhere [50].

3. Results and discussion

3.1. Analysis of the graphite-based materials

Table S2 summarizes the graphite-based materials employed in this study. Previous studies on catalytic ozonation by carbon-based catalysts have proposed the presence of π-extended aromatic structures and edges as active sites for O_3 activation towards the generation of ROS [53]. Considering the intrinsic nature of the graphite-based materials employed in this study, accessible sp^2 domains are proposed as active sites for the degradation reaction. A common strategy to evaluate the role of possible active sites in a catalyst is to mask them using post-synthetic modification methods and then evaluate the activity of the masked catalyst under similar conditions [53]. Thus, the accessible π-extended aromatic structure is considered as an active site for NG and was modified by a chemical oxidation with HNO_3 (NG-HNO_3) to randomly distribute oxygen functional groups. To confirm this chemical modification, combustion elemental analyses of the pristine NG and NG-HNO_3 were made and the observed analytical data confirmed a decrease in carbon content from 99 to 72.9 wt%. This chemical treatment may also modify other properties of NG (such as the specific surface area) and may also influence catalytic activity [53].

To obtain insights into the nature of these graphites, several analytical techniques were employed to establish their unique crystallographic, spectroscopic, physicochemical, textural, and morphological properties. Initially, a powder XRD of the solids was measured to better understand the crystal structures (Fig. 1a) [56–58,68]. All these samples exhibit a diffraction peak at about 26.6º which is a characteristic reflection (002) due to the plane of the aromatic graphene layers. Using Bragg's law ($n\lambda = 2d \sin\theta$) the interlayer d_{002} spacings of the graphites were estimated and these values are shown in Table 1. In general, the materials employed in this study exhibit similar interlayer distances (~ 3.35 Å) (Table 1) and characteristic diffraction patterns (Fig. 1a) that reflect their intrinsically graphitic nature [68,69].

Table 1 summarizes the microcrystallite parameters estimated from PXRD data (see experimental section) for the series of graphites and reveal significant differences. EG and EG600 solids exhibit the highest values for L_a, L_c, L, and the number of stacked layers. For the other graphite materials, the values of these parameters decrease in the order G>HSAG>NG~NG-HNO_3 (Table 1). The graphite-based materials (except NG-HNO_3) with the lowest stacking of the graphene layers ($N < 60$) are those solids with the highest specific surface areas namely, HSAG and NG and this is an important parameter that frequently determines catalytic activity.

In the area of heterogeneous catalysis, two important structural parameters that often largely determine the resulting activity are particle size and specific surface area [53]. The main explanation for these general observations is that the smallest particle size with the greatest surface area provides easy access for the reagents to the active sites, particularly when using two-dimensional layered materials (such as graphites). For catalytic ozonation processes using nanocarbon-based materials, the specific surface area has been highlighted as one of the critical parameters in determining their activity since the surface area facilitates ready access to the active sites (π-extended aromatic structures and edges) without significant mass transfer limitations [53]. Thus, the graphite-based materials used in this study are analyzed using HRSEM (Fig. 2, S2, and S3), isothermal N_2 adsorption-desorption measurements (Fig. S4) and the results are summarized in Table 1. There is

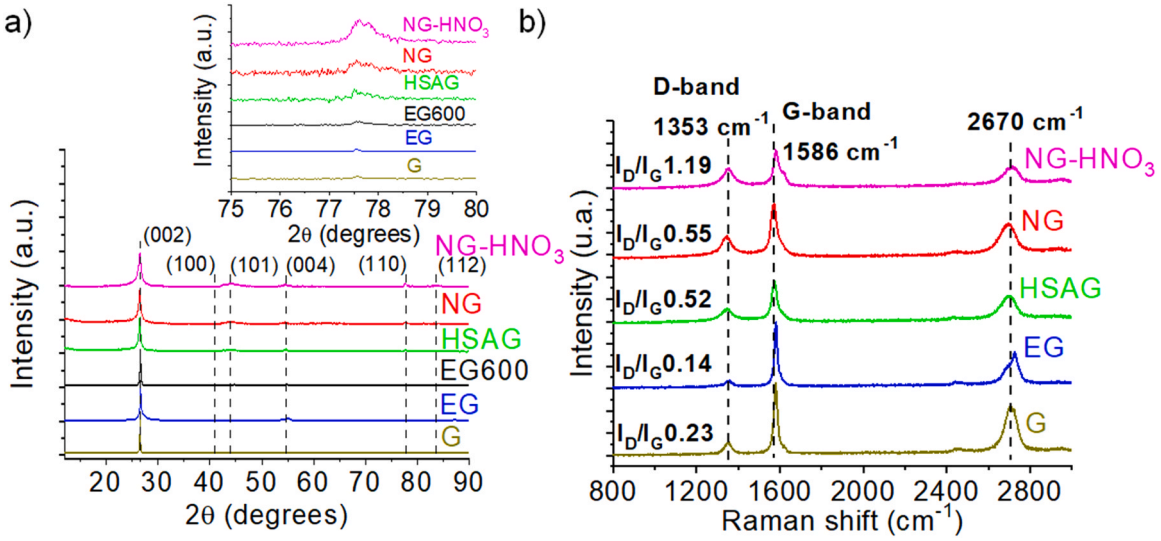

Fig. 1. (a) Powder XRD; and (b) Raman spectra of graphite-based materials.

Table 1
Summary of the PXRD data for the graphite-based materials.

Graphite-based solids	X-ray data	Microcrystallite parameter			Effective dimension of the crystallites (Å)	Average particle size (μm)	BET surface area (m^2/g)
	d_{002} (Å)	L_a (nm)	L_c (nm)	N	L		
G	3.3506	133	36	106	79	14	9
EG	3.3444	222	39	116	114	73	< 1
EG600	3.3483	222	40	118	115	19	~ 3
HSAG	3.3588	82	20	60	47	2.05	237
NG	3.3592	41	15	44	27	1.72	306
NG-HNO_3	3.3558	42	15	43	27	1.66	266

an inverse relationship between the average particle size and BET surface area. The sample with the smallest particle size corresponds to the highest surface area and vice versa. Previous studies have suggested that an important active site present in nanocarbons is the electron-rich and π-conjugated aromatic structure [53]. Thus, it is reasonable to conclude that the NG sample with the smallest particle size and the highest BET surface area would show the most activity.

The crystallographic and textural properties of the graphites were studied by PXRD, and the density of crystal defects in these samples were analyzed using Raman spectroscopy (results are shown in Fig. 1b). The Raman spectra reveal the presence of three main bands centered around 1353, 1586, and 2670 cm^{-1} which are characteristic of the D, G, and 2D bands, respectively [70]. The G band is a characteristic of defect-free graphites, while the D band corresponds to the disorder induced by the presence of structural defects and boundaries (Fig. S5). The density of structural defects in graphite-based materials is commonly estimated by the ratio I_D/I_G as a representative value for lattice disorder. In this study, the I_D/I_G ratio increases in the order EG<G<H-SAG<NG<NG-HNO_3. In Table 1 it can be observed that those graphites with the largest average particle sizes also have the lowest number of structural defects. Based on previous studies, the nature of the Raman D band observed for the graphites (with the exception of the NG-HNO_3 sample) is associated with the edges present in the samples [53]. The highest density of graphite edges relative to the basal plane is found in the NG sample. This observation correlates with the fact that NG exhibits the highest BET surface area and smallest particle size among the series of graphites and has the largest proportion of edges.

Previous studies suggest that the sample with the largest number of defects in the form of edges relative to the basal plane may also influence the ozonation catalytic activity of graphites [53]. Specifically, several studies have proposed that a key parameter favoring the O_3 activation towards ROS [47,53,71,72] is a high level of exposure to edging sites in nanocarbons. Additionally, other studies related to the use of graphenes as catalysts have proposed that the electron transfer process is faster at the edges than on the basal planes [73]. Therefore, it is reasonable that the graphitic samples used in this study that have large populations of edges with respect to basal planes exhibit relatively enhanced levels of activity. Based on the chemical oxidation preparation procedure, it is likely that the increase in defects (I_D/I_G) with respect to the parent NG is due to the presence of oxygen-functional groups within the structure. The observation of a new band at about 1640 cm^{-1} in the Raman spectrum of NG-HNO_3 suggests the presence of hydroxyl and carbonyl functional groups. FT-IR spectroscopy was further employed to analyze the oxygen functional groups in NG-HNO_3 (Fig. S6). In particular, NG-HNO_3 shows the presence of new vibration bands at about 3510, 1738, and 1248 cm^{-1} that suggest –OH, C═O and C-O functionalities, respectively. Furthermore, NG-HNO_3 also exhibits new bands at about 2980 and 2900 cm^{-1}, which together with 1390 cm^{-1}, indicate $–CH_2$ groups.

Thermogravimetric analyses (TGA) of the graphitic samples under an oxygen atmosphere were made to study their thermal stability. The plots in Fig. S7 show that this stability decreases in the order G~EG600 >HSAG>NG>EG. The lowest level of thermal stability of EG in the series starts to degrade at about 200 °C and is associated with the expansion of the graphene layers intercalated with sulfate anions [61]. EG600 exhibited a notable increase in thermal stability and reached a similar level to the G sample. The relatively lower level of thermal stability of NG and HSAG when compared to the most stable G seems to correlate with the increase in defects (I_D/I_G ratio) shown in the Raman spectra, as well as the increase in BET surface area, and the decrease in particle size (Table 1). However, the correlations observed for G, HSAG, and NG are not applicable to the EG sample as it shows the lowest level

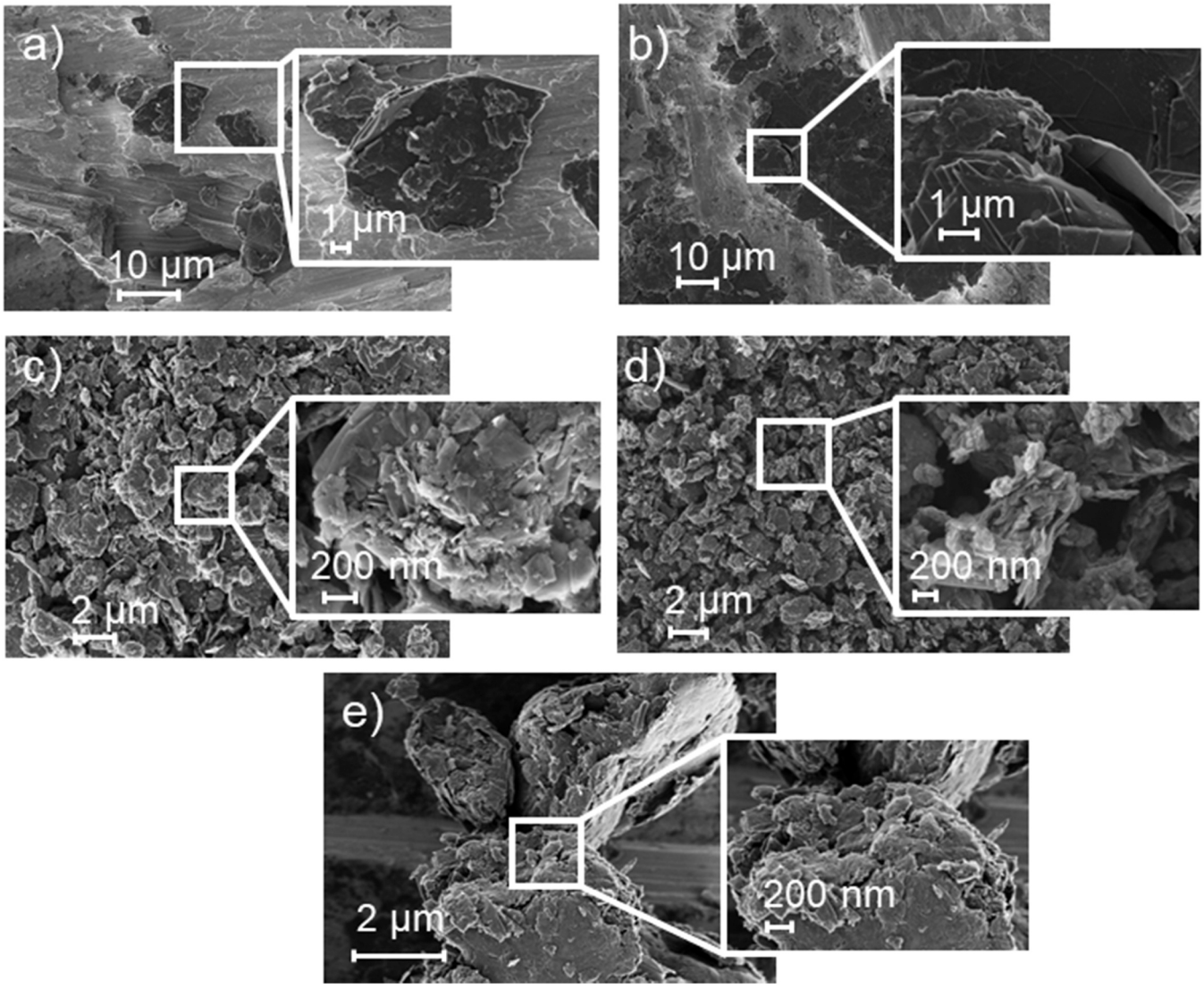

Fig. 2. HRSEM images of (a) G, (b) EG, (c) HSAG, (d) NG, and (e) NG-HNO_3.

of thermal stability, the lowest degree of defects (I_D/I_G ratio), the smallest surface area, and the largest particle size. TGA also shows that the thermal stability of NG-HNO_3 is relatively lower than pristine NG. This observation supports the existence of oxygen functionalities within the NG-HNO_3 sample that thermally decompose at temperatures above 300 ºC [74].

3.2. Catalytic activity

The catalytic performances of the graphite-based solids were evaluated as ozonation catalysts for degrading oxalic acid in water. Control experiments revealed that the adsorption of oxalic acid over graphite-based materials is below 2% at pH 3. As shown in previous studies,

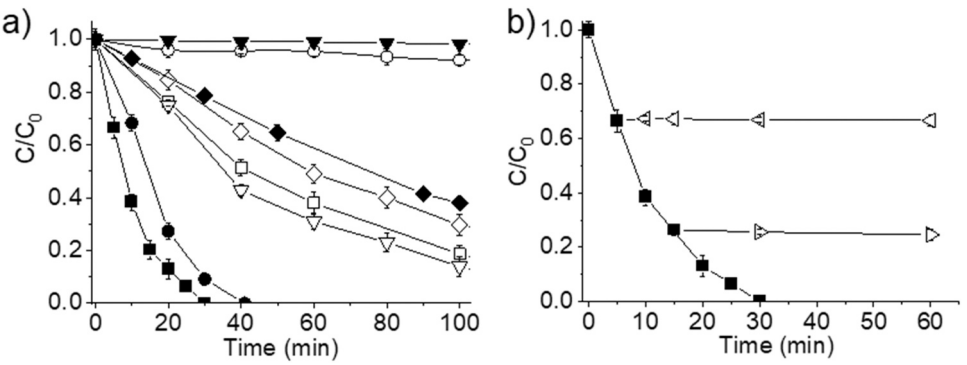

Fig. 3. (a) Metal-free catalytic ozonation of oxalic acid (50 mg/L), catalyst (100 mg/L), pH 3, 20ºC, and O_3 inlet to the glass reactor (150 mg/h). Legend: ozone (▼), EG (○), NG-HNO_3 (◆), EG600 (◇), G (□), AC (▽), HSAG (●), and NG (■). (b) NG (■), NG filtrated at 5 min (◁) and NG filtrated at 15 min (▷).

oxalic acid cannot be degraded using only O_3 under similar reaction conditions [29,30]. Fig. 3a shows that all the graphite-based materials in the series are active for ozone activation and oxalic acid degradation. The results indicate that NG exhibits the highest level of catalytic activity (100%, 30 min) in the series, followed by HSAG (100%, 41 min), G (82%, 100 min), EG600 (61%, 100 min), NG-HNO_3 (62%, 90 min) and EG (8%, 100 min). The heterogeneous behavior of the catalyst was evaluated before analyzing the reasons for the high level of NG catalytic activity in comparison with the other samples. One common strategy for this evaluation is to remove the solid catalyst from the reaction medium once the reaction has started and to observe the progress of the reaction in the absence of the catalyst under identical conditions. The solid catalyst was removed when conversions reached around 30% and 65%. The liquid without catalyst was allowed to react under similar ozonation conditions and the complete inhibition of the oxalic acid degradation was observed. These experiments are shown in Fig. 3b and confirm the occurrence of catalytic ozonation in a truly heterogeneous fashion. Importantly, NG shows greater levels of catalytic activity (100%, 30 min) than commercial Co_3O_4 (100%, 80 min) often used as a benchmark transition metal-based ozonation catalyst under the same reaction conditions (see Fig. S8).

To rationalize the observed catalytic activity for these materials, the physico-chemical and textural properties of the materials were analyzed. Among these solid catalysts, the least active sample was EG and this is due to its lowest BET surface area (< 1 m^2/g) and largest particle size (Table 1). Interestingly, EG600 was more catalytically active (Fig. 3a), despite having a relatively higher surface area (~3 m^2/g), a lower stacking of graphene layers, and a similar microcyrstallite parameter with respect to the parent EG (Table 1). The activity performance of G (82%, 100 min) was greater than EG600 (61%, 100 min) and this is attributed to its relatively greater surface area (9 m^2/g), smaller average particle size (14 vs 19 μm), and lower graphene stacking. The use of HSAG produces significantly greater catalytic activity (100%, 41 min) and this is due to a higher BET surface area (237 m^2/g), much smaller particle size (2.05 μm), and lower graphene stacking compared to G (Table 1). In good agreement with these observations, the greater catalytic activity of NG compared to HSAG (which has a similar particle size) can be explained by its higher BET surface area (306 m^2/g), lower graphene layer stacking, and slightly smaller (but still significant) particle size (1.72 μm). Remarkably, the catalytic activity achieved with NG (100%, 30 min) is relatively greater than the commercially available AC (86%, 100 min) used as a benchmark metal-free ozonation catalyst, despite having a greater BET surface area (~880 m^2/g) [75]. In accordance with these correlations, the catalytic data observed for the series of graphite-based materials show a direct relationship with defects (I_D/I_G ratio). Among these samples, NG has the largest number of defects and the highest level of activity.

Furthermore, the level of catalytic activity by NG-HNO_3 is much lower than NG. NG-HNO_3 has a smaller BET surface area (266 m^2/g) than the NG sample (306 m^2/g) and this can partially explain the decreased activity. Further, it should be noted that although the NG-HNO_3 area is much larger than EG600 (3 m^2/g) or G (9 m^2/g), its catalytic activity level is lower. These results together with previous analytical data are interpreted considering lower proportion of active sites (π-extended aromatic structures and edges) in NG-HNO_3 had partially degraded compared to NG, and, therefore the catalytic activity had also decreased.

These comparison data highlight the importance of using NG with a graphitic nanosized structure with the highest population of edges even though it has a relatively smaller BET surface area (306 m^2/g) than the highly porous AC (880 m^2/g) and its amorphous structure with both graphitic and sp^2 domains as well as several oxygen functional groups (C:O molar ratio of 4.5) [75]. Moreover, a previous study has shown the inactivity of the sp^3 domain in graphitized nanodiamonds.[50].

Factors such as the dispersibility of graphites and the adsorption behavior of oxalic acid were studied in addition to the BET surface area of graphites. The presence of small particles of graphites may favor higher dispersibility in water and so facilitate the catalytic ozonation process by increasing the physical contact between these graphites and O_3 and/or $^1O_2$ (see Section 3.4). To obtain further insights regarding this process, graphite suspensions were prepared in water at 100 mg/L as in the case of the catalytic ozonation experiments. UV-Vis absorption analyses of these graphite suspensions at times 0 and 6 h showed that the order of dispersibility (Fig. S9a) matches with the order of catalytic activity. Therefore, for the graphite-based materials, the catalytic activity achieved is related to a high surface area with a sp^2 domain able to decompose O_3 to $^1O_2$ and a further interaction of $^1O_2$ with the graphites (see Section 3.4). The dispersibility of the materials also favored these interactions. In addition, graphite-based materials were used to adsorb oxalic acid in water at pH 3. Fig. S9b shows that the order of oxalic acid adsorption agrees with the catalytic ozonation order observed earlier.

One of the challenges in AOPs is to develop catalytic systems that can operate across a broad range of pH values. For this reason, the performance of an NG sample was also studied as a function of the initial pH for oxalic acid degradation (Fig. 4a). For the sake of comparison, the performance of HSAG was considered under identical reaction conditions (Fig. 4b). Some studies have shown that O_3 concentration decreases as the pH of the solution increases [11,48] and others have reported that a reaction between O_3 and HO^- forms hydroxyl radicals [11]. The lower level of catalytic activity observed with NG for oxalic acid degradation in water at basic pH is attributed to a lower O_3 concentration interacting with the catalyst to form ROS. The use of HSAG results in less degradation in water for all pH values studied from 3 to 11 in comparison with the most active NG sample. Interestingly, the activity of NG is even higher at a pH value of 11. Previous related studies with edged-hydroxylated HSAG (HSAG-OH) [48] and graphitized nanodiamonds [50] showed limited activity at neutral or basic pH values for the degradation of oxalic acid in water. The superior performance of NG compared to HSAG across the pH range under study further confirms the importance of a nanosized graphitic structure with the highest population of edges as well as a high surface area.

3.3. Catalyst stability

One important issue in catalysis is catalyst stability and this is often assessed by performing reusability experiments [32,76]. This is of special importance in metal-free heterogeneous catalysis for AOP application due to the formation of highly active ROS during the process that can interact with the catalyst [11]. For this purpose, the most active NG sample was submitted to consecutive reuse experiments at pH 3. Fig. 5a shows that NG can be effectively reused for five cycles with only a slight decay in activity and complete degradation occurs after some additional minutes of reaction. The times required for complete oxalic acid degradation were 30, 35, 40, 45 and 45 min for 1st, 2nd, 3rd, 4th, and 5th reuses, respectively. Based on knowledge from previous studies involving carbon-based materials as ozonation catalysts, it is believed likely that the slight observed decay may be explained by the partial oxidation of NG [48,49]. Thermal annealing under an argon atmosphere is a common strategy for heterogeneous solids to recover most of the initial catalytic activity in carbon materials. The purpose of this thermal annealing is to accelerate the decomposition of the oxygen functional groups and re-graphitize the carbocatalyst. With this knowledge, six-times used NG (NG-6U) was submitted to a pyrolysis under an argon atmosphere at 1100 ºC for 1 h to obtain NG-6U-REG. Interestingly, the catalytic activity of the NG-6U-REG was restored and could be employed for five additional consecutive catalytic cycles with only a minor decay in activity.

To learn more about partial catalyst deactivation and re-activation processes, a comparative analysis of the fresh, NG-6U, and NG-6U-REG materials was made using several techniques. Although the PXRD (Fig. 5b) of these three samples reveals similar patterns, a more detailed investigation shows small but significant changes in the microcrystallite

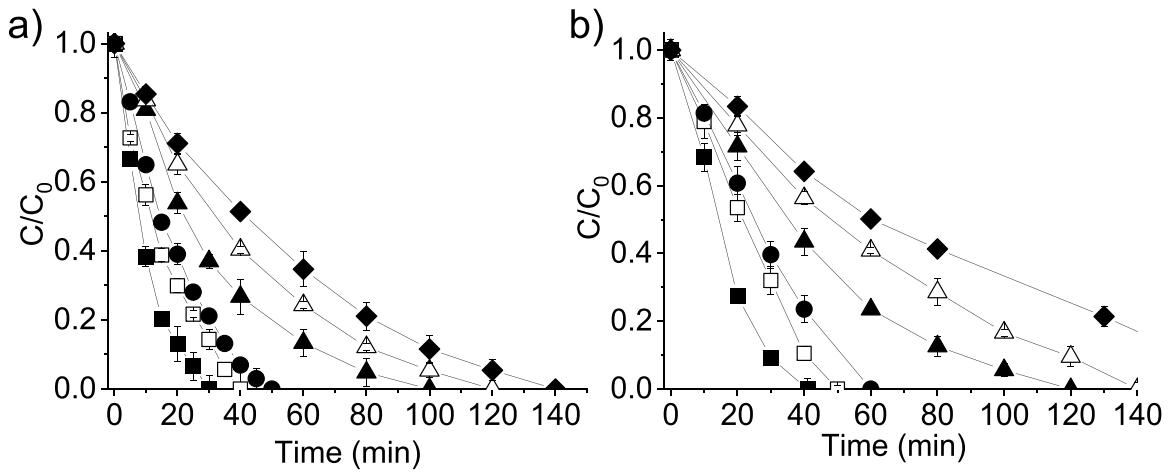

Fig. 4. Influence of initial pH values using NG (a) and HSAG (b). Legend: pH 3 (■), pH 4 (□), pH 6 (•), pH 8 (▲), pH 10 (△) and pH 11(◆) under identical conditions as shown in Fig. 3.

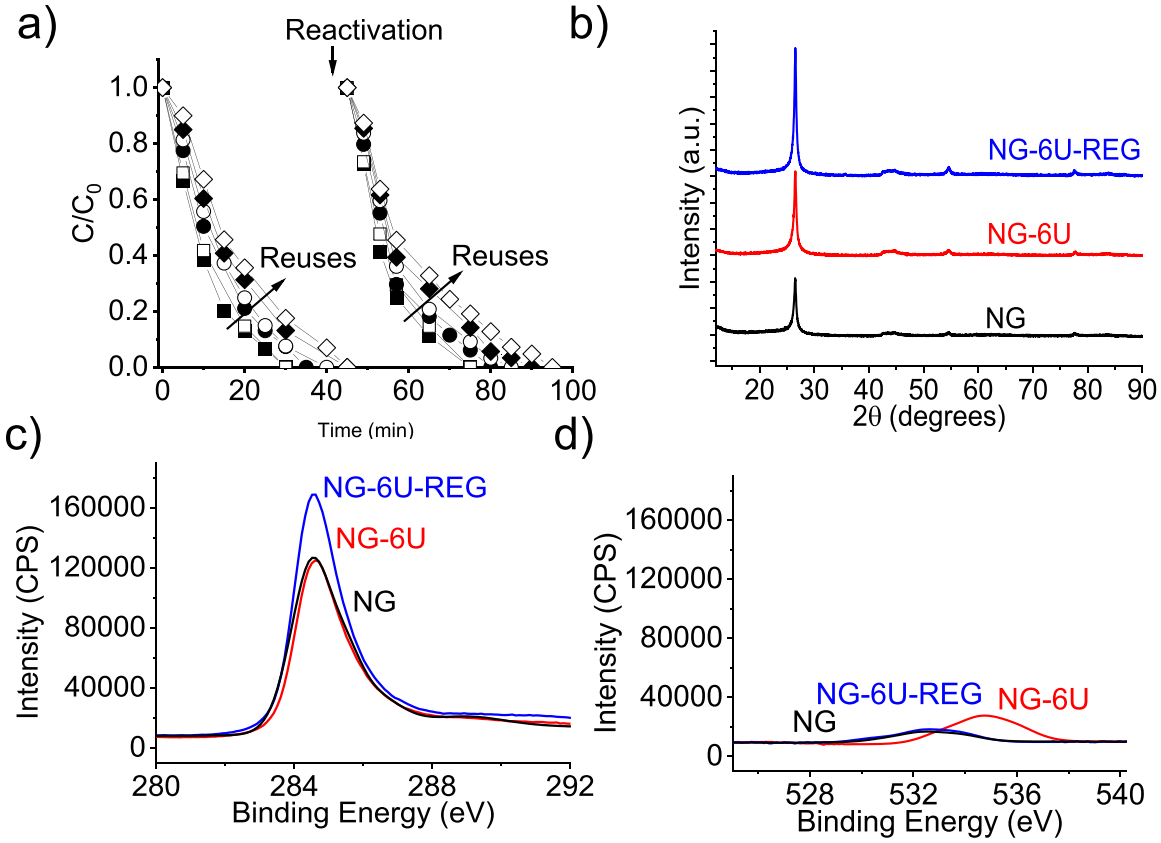

Fig. 5. (a) Reusability and reactivation of NG solid under the conditions reported in Fig. 3. Legend: 1 st use (■), 2nd use (□), 3rd use (•), 4th use (○), 5th use (◆), 6th use (◇). (b) PXRD (c) XPS C 1 s (c) and (d) XPS O 1 s of NG, NG-6U and NG-6U-REG.

parameters. In particular, the NG-6U sample shows a slightly higher L_c parameter (17 nm) with respect to the fresh sample (15 nm), while the regenerated NG-6U-REG recovers its original value. This observation is correlated with the partial oxidation of the graphene layers of NG after six uses with the concomitant expansion of the layers. A thermal regeneration of NG-6U resulted in a re-graphitization of the sample and contraction of the graphene layers so that it resembled the pristine sample. Combustion elemental analyses showed that the used NG-6U sample had less carbon (92.4 wt%) than the fresh NG sample (> 97%), while the initial carbon content was restored in the NG-6U-REG sample. A TGA analysis was made for the fresh, used, and regenerated samples. Fig. S10 shows that the NG-6U solid is less thermally stable than the fresh NG sample. These results correlate well with the partial oxidation of NG-6U with oxygen functional groups that can be thermally decomposed from about 250–700 °C. Interestingly, the NG-6U-REG sample showed a level of thermal stability similar to the fresh NG catalyst. Additionally, the NG-6U sample had a slightly smaller BET surface area (298 m^2/g) (Fig. S11) than the NG sample (306 m^2/g) (Table 1). Furthermore, the NG-6U-REG sample (Fig. S11) recovered its original BET value as in the case of NG solid.

The three samples were further analyzed with XPS and Raman spectroscopies to gain more information about these observations. Investigation of the XPS C 1 s and O 1 s spectra of the NG-6U and NG indicate that the former shifted to higher binding energies (Fig. 5c, d). In addition, the XPS O 1 s spectrum of NG-6U showed a higher signal intensity than the fresh NG sample. In fact, quantitate XPS C 1 s and O 1 s analyses show that the NG-6U sample contained more oxygen (~ 8 wt%) than the fresh sample (~3 wt%). XPS O 1 s deconvolution of NG-6U further confirms the partial oxidation of the NG-6U catalyst with hydroxyl (533.1 eV), carbonyl (534.2 eV), or carboxylate (536 eV) groups (among other possibilities) (see Fig. 5 and S32). Remarkably, the C 1 s and O 1 s spectra of the NG-6U-REG sample resembles the fresh NG sample (Fig. 5). Specifically, the XPS O 1 s of NG-6U-REG show that the carboxylate groups were removed due to their instability at 1100 °C [74]. Furthermore, Raman spectroscopy (Fig. 6a and S13) showed an increasing I_D/I_G ratio for the NG-6U sample (0.75) with respect to fresh NG (0.55). The thermally annealed NG-6U sample enables largely restoring the defect density (I_D/I_G 0.6) when compared to the parent sample. These XPS and Raman results confirm that a thermal pyrolysis treatment of the partially oxidized NG-6U sample is an appropriate strategy for largely restoring the initial graphitic structure.

Additionally, a comparative solid-phase EPR measurement for NG, NG-6U, and NG-6U-REG samples was performed (Fig. S14). The results show that the NG-6U sample, due to partial oxidation of its graphitic structure, exhibits an EPR signal attributable to the presence of unpaired electrons like dangling bonds. Interestingly, the NG and NG-6U-REG samples are EPR silent [77].

Electron microscopy techniques were also employed to analyze the fresh NG and NG-6U samples during the catalytic ozonation process and after thermal regeneration. HR-SEM measurements of the three samples under study reveal no significant morphological changes (Fig. S15). TEM analysis (Fig. 6b-d and Fig. S16) of the fresh NG confirms an expected graphite interlayer distance of about 3.35 Å (corresponding to the 002 plane as observed in XRD). The NG-6U sample also reveals interlayer distances of 3.35 Å, with some domains showing interlayer distances of about ~2.2 Å. The formation of these domains can be explained by the partial transformation of sp^2 to sp^3 carbons due to the partial oxidation of graphene layers in NG during catalytic ozonation. Reactivation of the NG-6U sample by thermal pyrolysis results in a NG with interlayer distances of 3.35 Å. These conclusions are in full agreement with previous analyses of the fresh NG, NG-6U, and NG-6U-REG samples using combustion elemental analyses, XPS, and Raman techniques.

The above comparative data for the NG, NG-6U, and NG-6U-REG samples confirm that the slight decrease in catalytic activity during the reuse experiments using NG as a catalyst can be attributed to partial oxidation and, therefore, decrease of the population of actives sites. These data, together with the observed drop of activity of the NG-HNO_3 sample when compared to the parent NG, support the attribution of an electron-rich π-extended aromatic structure and the edges of NG as active sites. In addition, the pyrolysis of NG-6U is shown to be an appropriate method for recovering both the graphitization of NG and its initial catalytic activity.

The catalytic activity, stability, and durability of NG was further assessed with the use of relatively small amounts of catalyst (20, 50, or 100 mg/L) to efficiently degrade high concentrations of oxalic acid in

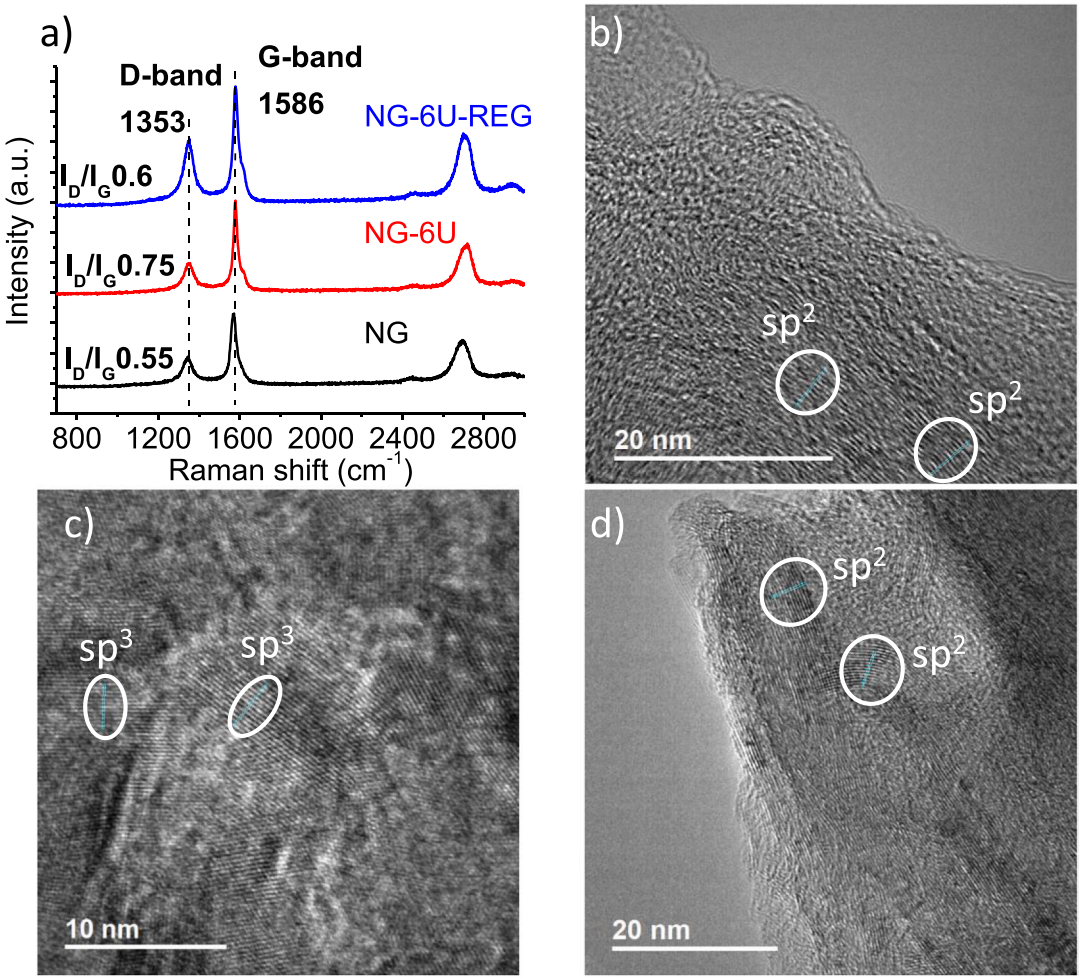

Fig. 6. (a) Raman and HR-TEM images of (b) NG, (c) NG-6U and (d) NG-6U-REG.

water (1 g/L) (Fig. 7). In one of the previous examples, HSAG-OH as a metal-free heterogeneous catalyst (50 mg/L) degraded 1 g/L of oxalic acid in water at pH 3 in 17 h (Table S3). Under similar reaction conditions, NG completely degrades oxalic acid in about 11 h, thus showing superior catalytic activity than HSAG-OH (Table S3). Furthermore, 20 mg/L of NG was sufficient to degrade oxalic acid with a concentration of 5000 mg/L in water (Fig. 7). Table S3 also shows that NG is a highly active and stable metal-free ozonation catalyst in terms of reusability compared to hybrid sp^2/sp^3 nanodiamonds, as well as reduced graphene oxide (rGO), and other related carbon-based catalysts under similar reaction conditions [46–50,52,78]. Overall, a comparison of NG activity with other reported carbon-based solids firmly suggests that the achieved degradation performance and stability of NG ranks it as the most efficient metal-free ozonation catalyst reported until now (Table S3).

3.4. Reaction mechanism

A common strategy to address the existence of ROS is to employ scavengers during the measurement of catalytic activity. *t*-Butanol ($5{\cdot}10^8$ M^{-1} s^{-1}) [27] and DMSO ($4.2{\cdot}10^9$ M^{-1} s^{-1}) [79] have been frequently used as selective hydroxyl radical scavengers in solution; and methanol ($7{\cdot}10^8$ M^{-1} s^{-1}) [80] is used as a hydroxyl radical scavenger in both bulk and solution. However, the reactivity of O_3 with *t*-butanol ($3{\cdot}10^{-3}$ M s^{-1}), [27] DMSO (0.4162 M^{-1} s^{-1}) [81], or methanol (0.024 M s^{-1}) [31], is negligible when compared to that observed with hydroxyl radicals. Fig. 8a shows the influence of scavengers in the degradation of oxalic acid in water with NG as a metal-free ozonation catalyst. These data indicate that the addition of *t*-butanol, DMSO, and methanol do not alter catalytic degradation. These observations directly indicate the absence of hydroxyl radicals. Similarly, the generation of superoxide/hydroperoxide radicals during catalytic ozonation was ruled out based on the use of *p*-benzoquinone as a scavenger [82]. In contrast, the observed partial oxalic acid inhibition with NG in the presence of NaN_3 ($k_{^1O2/NaN3} = 2.2{\cdot}10^9$ M s^{-1}) [83] or furfuryl alcohol (FFA) ($k_{^1O2/FFA} = 1{\cdot}10^8$ M s^{-1}) [84] may be attributed to the presence of $^1O_2$ as ROS. Similar conclusions were obtained using DMSO (Fig. S17), *p*-benzoquinone (Fig. S18), and NaN_3 (Fig. S19) as radical quenchers during oxalic acid degradation for the graphite-based materials (G, EG, EG600 and HSAG).

Previous studies have reported that the rate of O_3 decomposition in water can be correlated with the generation of ROS during the catalytic ozonation [46]. Fig. 8b shows that the order of O_3 decomposition in water at pH 3 with graphite-based solids agrees with the order observed for oxalic acid decomposition under the same reaction conditions. These results together with the above quenching experiments can be associated with the presence of $^1O_2$ during the catalytic ozonation process.

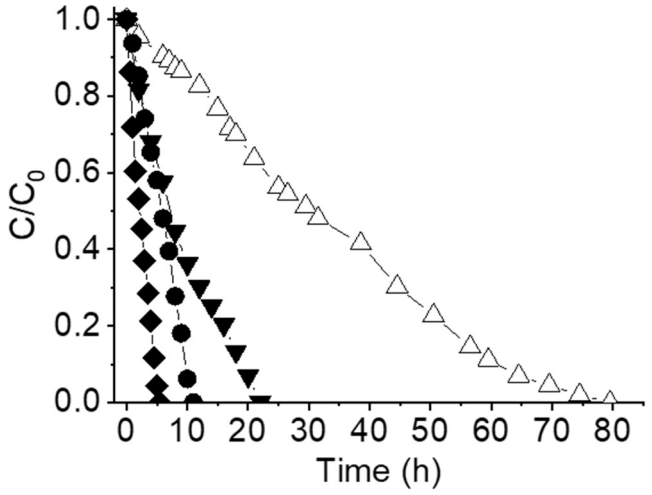

Fig. 7. Carbocatalytic activity for the degradation of a relatively large amount of oxalic acid (1 g/L) in water at pH 3 using NG at 20 (▼), 50 (●) or 100 (◆) mg/L catalyst or oxalic acid (5 g/L) using 20 mg/L catalyst (△).

EPR measurements were performed to further confirm the generation ROS during the carbocatalytic activation of O_3 using the series of graphite-based materials. In particular, the use of TEMP (Fig. 8c) as a spin trap during the catalytic ozonation resulted in the formation of the TEMPO adduct that showed a characteristic three lines of the same intensity with a coupling constant 17.3 G.[85] Interestingly, the order of the EPR intensity signals observed for TEMPO formation with the series of graphites matches the order for oxalic acid degradation.

To further detect other ROS species, DMPO was employed as a selective spin trap for the $HO^{\cdot}$ and/or $O_2^{\cdot-}/HOO^{\cdot}$ radicals. The results show that all these samples formed DMPOX (Fig. 8d). These EPR measurements together with selective quenching experiments conclude the absence of $HO^{\cdot}$ and/or $O_2^{\cdot-}/HOO^{\cdot}$ during catalytic ozonation. Regardless of these observations, Fig. 8d shows that the EPR intensity of the DMPOX signal using the graphite solids also follows the order of activity observed for oxalic acid degradation. The use of O_3 in the absence of a catalyst also resulted in the formation of DMPOX. These results agree with previous studies reporting the oxidation of DMPO to DMPOX either by $^1O_2$ [86,87] or O_3 [88]. Furthermore, the use of N-*tert*-butyl-α-phenylnitrone (PBN) to detect $HO^{\cdot}$ and/or $O_2^{\cdot-}/HOO^{\cdot}$ radicals with NG did not reveal any EPR signals.

Based solely on the detection of $^1O_2$ during catalytic ozonation, we further explore its role for oxalic acid degradation using graphites. Initially, the possibility was evaluated of $^1O_2$ degrading oxalic acid in the absence of NG. Based on previous studies, Rose Bengal was used as a photosensitizer to generate $^1O_2$ in water at pH 3. In good agreement with previous studies [89], the UV-Vis irradiation of Rose Bengal in water at pH 3 in the presence of TEMP forms TEMPO as revealed by EPR measurements following the generation of $^1O_2$ (Fig. S20a). Subsequently, a control experiment showed that the irradiation of the oxalic acid solution in the absence of a catalyst cannot degrade oxalic acid in water at pH 3 (data not shown).

Interestingly, analogous photocatalytic experiments using Rose Bengal in the presence of a series of graphites resulted in the degradation of oxalic acid (Fig. S20b). These data indicate that $^1O_2$ and NG interact in such a way that favors the degradation of oxalic acid. Furthermore, the order of activity obtained during oxalic acid degradation via photosensitized $^1O_2$ production in the presence of graphites follows the same order of activity as catalytic ozonation. Overall, these experiments show the important role of graphites in the degradation of oxalic acid with the presence of O_3 or $^1O_2$.

Previous studies have proposed that the graphitic basal plane and edges of several nanocarbons act as active sites during catalytic ozonation [53]. This electron-rich and highly conjugated π-extended aromatic structure can favor electrophilic binding to O_3 that can later be dissociated into ROS and/or the formation of an O_3-carbon complex. We also believe that the superior activity of NG is due to its ability to efficiently transform O_3 to $^1O_2$. , $^1O_2$ can interact with the accessible active sites in NG favoring the degradation of oxalic acid.

3.5. Influence of inorganic ions and humic acid

An important consideration when developing heterogeneous ozonation catalysts is the possible influence of the common ions present in water [31]. There are many reports in the literature about the influence of inorganic anions frequently found in natural water (such as chlorides, phosphates, sulfates, carbonates, and nitrates) which act as scavengers of the ROS similarly to $HO^{\cdot}$ radicals generated during catalytic ozonation of water pollutants [31]. This situation hampers the efficient application of these catalytic ozonation systems in natural water matrixes. Based on these precedents, this study investigates the influence of inorganic anions (phosphates, carbonates, sulphates, nitrates, and chlorides) that are

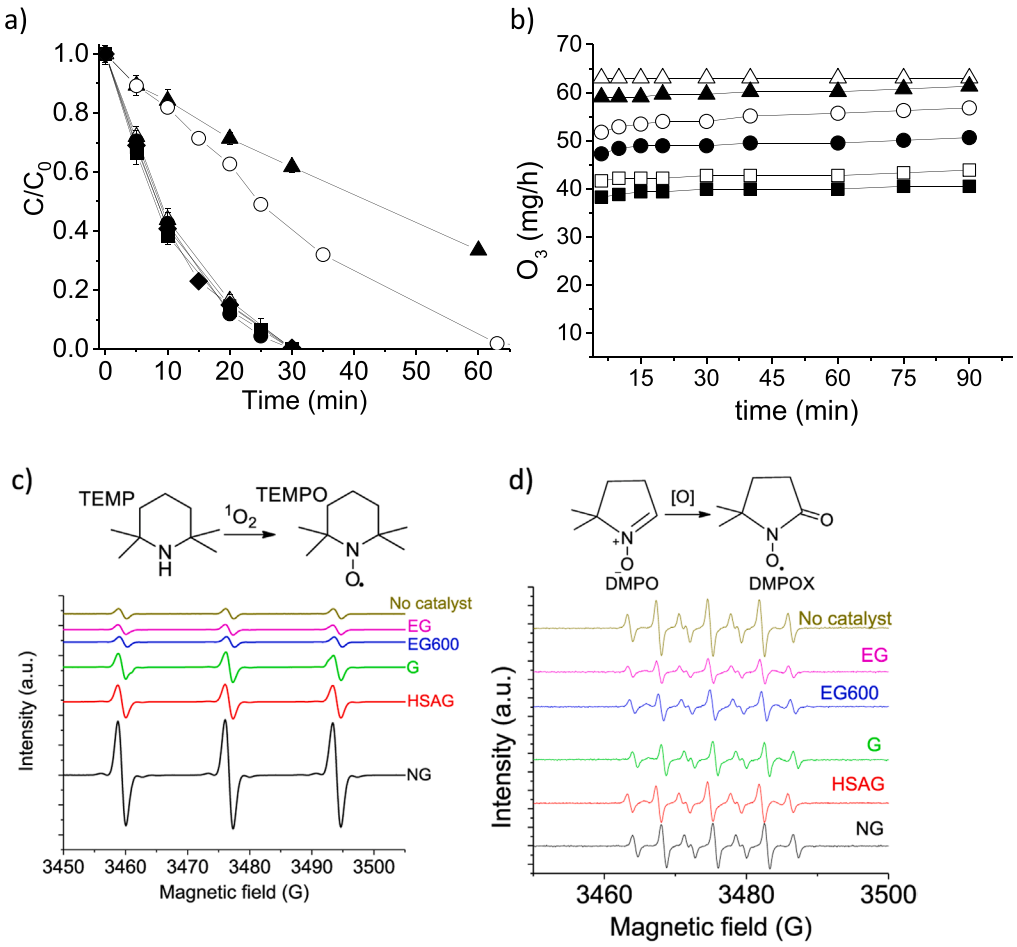

Fig. 8. (a) Influence of ROS scavengers on the catalytic performance of NG under identical conditions to Fig. 3 without (■) or with NaN_3 (▲), furfuryl alcohol (○), DMSO (□), *t*-butanol (△), methanol (•) and *p*-benzoquinone (◆); (b) O_3 amount (mg/h) measured at the exit of the glass reactor containing 200 mL of water at pH 3 in the absence (△) or in the presence of EG (▲), EG600 (○), G (•), HSAG (□), and NG (■). Note: O_3 inlet is 150 mg/h. EPR spectra recorded with (c) TEMP and (d) DMPO in the absence or presence of graphite-based materials as indicated during ozonation.

commonly found in natural waters on the activity of NG (Fig. 9a and S21). In general, these inorganic anions at concentrations that can be found in natural water (50 or 200 mg/L) have only a minor influence on the resulting catalytic activity during the metal-free ozonation of oxalic acid with NG at pH 7. Furthermore, the presence of chloride at concentrations commonly found in seawater with values as high as 30 g/L has a negligible influence during oxalic acid ozonation with NG as a solid catalyst (Fig. S21). ROS generation during catalytic ozonation using NG may explain the low level of influence of these inorganic ions on catalytic activity. As it has been demonstrated with EPR measurements and selective quenching experiments, $^1O_2$ is the only ROS generated in the catalytic system and neither hydroxyl nor superoxide/hydroperoxide species have been detected. Therefore, the minor influence of these inorganic ions may be associated with the absence of $HO^{\cdot}$ and/or $O_2^{\cdot-}/HOO^{\cdot}$ species. Regardless of these comments, Fig. 9a shows that the presence of phosphate ions has a minor but significant influence on catalytic activity compared to carbonates/bicarbonates that have almost no influence. A recent study reported that the self-decay kinetics of O_3 in an aqueous solution are faster in the presence of phosphate ions than carbonates [90]. Therefore, this study proposes that the observed influence of phosphate ions during the catalytic ozonation of oxalic acid with NG is also due to a similar process. Other studies have reported that chloride ions can react with O_3 to form hypochlorous/hypochlorite species in such a way that the effective concentrations of O_3 that participate in the degradation of oxalic acid are lower (although under the present reaction conditions this process seems to have negligible influence) [91]. Other factors such as the increase in ionic strength of water due to the presence of inorganic ions may also influence the catalytic ozonation by varying the mass transfer rates between the solid catalyst and the pollutant in the water and the O_3 cannot be discharged.

In addition to the influence of inorganic anions, naturally occurring organic matter can also react with the generated ROS during catalytic ozonation [92]. A common strategy to evaluate the effect of natural organic matter in the laboratory is to use commercially available humic acid as a reference [92]. In this study, the catalytic ozonation of oxalic acid with NG is evaluated in the presence of different concentrations of humic acid in water. Fig. 9b shows that the presence of increased concentrations of humic acid in water from 1 to 2 mg/L delays the full degradation of oxalic acid. These observations can be attributed to a combination of several factors. The O_3 supplied to the reaction can react with humic acid as reported [93] and so decrease the amount of ozone available to be catalytically decomposed by NG to ROS. However, the catalytically formed ROS using NG may react with humic acid and so decrease its availability to degrade oxalic acid in water. Other factors such as adsorption of humic acid by NG may also hamper ozone activation to ROS and so decrease the resulting catalytic activity of the carbocatalyst.

3.6. Activity of NG in natural water matrixes

Factors that frequently limit a cost-effective application of catalytic AOP in water are naturally occurring inorganic ions (anions or cations) and organic matter [31,92]. The development of transition metal-based [11,12,24] or metal-free [53] heterogeneous ozonation catalysts for degrading water pollutants has been widely reported. Less attention has been given to evaluate the performance of these heterogeneous ozonation catalysts in natural water matrixes [26]. This study also aims to examine the potential of NG as a metal-free ozonation catalyst for application in natural waters. For this purpose, a catalytic ozonation

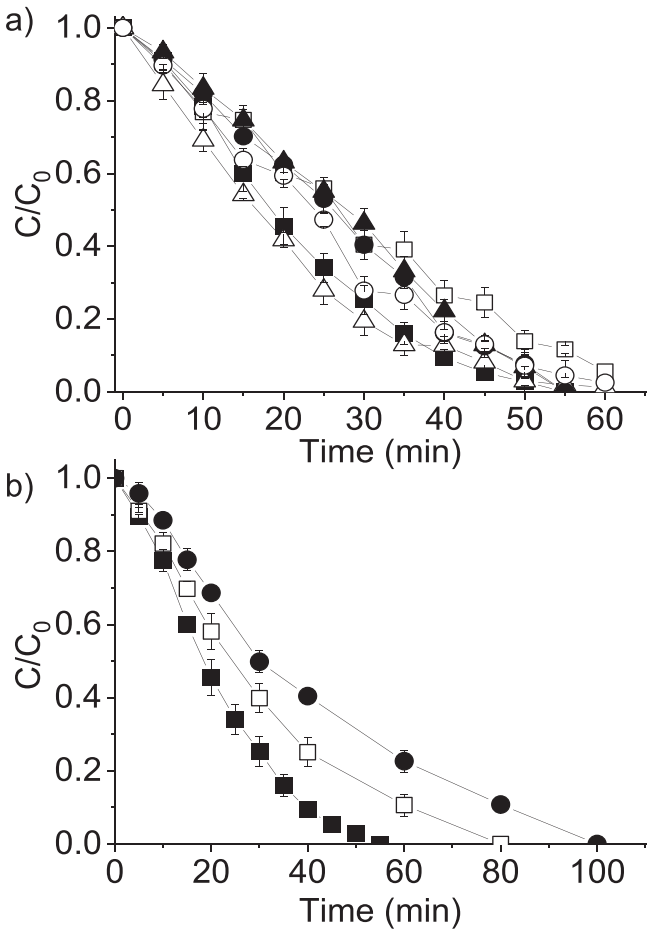

Fig. 9. (a) Ozonation of oxalic acid at pH 7 using NG without (■) or with inorganic ions. Legend: NaH_2PO_4 (□), Na_2SO_4 (▲), $NaHCO_3$ (△), $NaNO_3$ (•) and NaCl (○) at 50 mg/L. (b) ozonation of oxalic acid at pH 7 using NG without (■) or with humic acid at 1 mg/L (□) and 2 mg/L (•).

using NG for the degradation of oxalic acid in two natural aquatic sources: surface river water (Turia River, Valencia, Spain) and a Mediterranean seawater (Valencia, Spain) was performed. The sample from the Turia River was collected just upstream from a water treatment plant that supplies drinking water to more than 1.5 million residents in Valencia. The Mediterranean seawater was collected from the Malvarrosa beach in the city of Valencia. Table S1 shows some of the common physicochemical and microbiological water quality parameters for surface river and Mediterranean seawater, respectively. Fig. 10 shows that the degradation of oxalic acid in both waters can be carried out effectively with reaction times that are longer than analogous experiments using Milli-Q water. Based on the negligible influence of inorganic ions on the observed NG catalytic activity for oxalic acid degradation in Milli-Q water, the longer time required for its degradation in the natural waters under study can be attributed to the presence of natural organic matter and/or microorganisms in both waters. It is interesting to consider that previous studies showed the quenching of highly aggressive hydroxyl radicals is largely due to the presence of inorganic anions, especially CO_3^{2-} or humic acid [26]. Therefore, the use of NG as an ozonation catalyst results in the formation of ROS (such as $^1O_2$) rather than hydroxyl radicals and this may partially explain the relatively good performance observed for oxalic acid degradation in natural water matrixes. Overall, the results obtained in this study highlight the potential use of NG as a metal-free ozonation catalyst using natural water matrixes such as surface river or seawater.

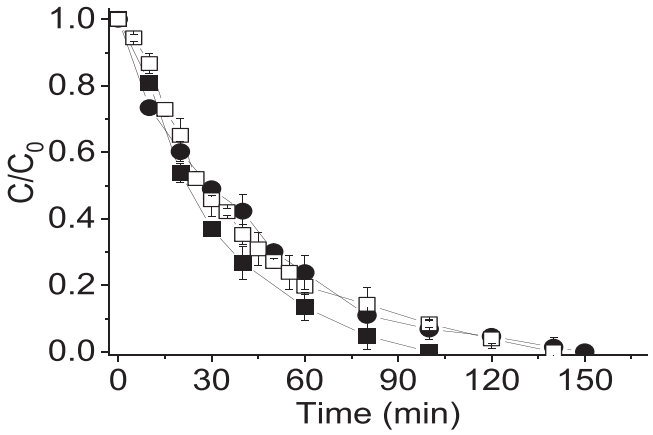

Fig. 10. Ozonation of oxalic acid (50 mg/L) at pH 8 using NG (100 mg/L) in natural water matrixes. a) Legend: distilled water at pH 8 (■), Turia River (□), seawater (•).

4. Conclusions

This study shows that NG is a highly efficient and durable catalyst. The catalytic activity achieved with NG is greater than that achieved with traditional graphite-based materials such as G, EG, EG600, and HSAG as well as benchmark carbonaceous solids such as AC or Co_3O_4. Analysis of the tested graphite-based materials revealed their unique crystallographic, spectroscopic, physicochemical, textural, and morphological properties. These data together with the observed order of activity NG>HSAG>G>EG600 >EG suggest that the activity of NG is attributable to its unique nanosized graphitic structure, large population of defects such as edges, high surface area, good dispersibility and adsorption capacity. After several uses, NG retains most of its initial catalytic performance, however, a partially deactivated sample (NG-6U) can be restored with a thermal treatment at 1100 ºC. Data from analyses of the NG, NG-6U, and NG-6U-REG solids indicate that the main reason for catalyst deactivation is partial oxidation; and a thermal regeneration treatment enables a recovery of most of the initial graphitic structure and catalytic activity. In addition, productivity tests indicate that large amounts of oxalic acid as an organic model pollutant (5000 mg/L) can be fully degraded using relatively small amounts of NG as catalyst (20 mg/L). These catalytic activity and stability data enable us to conclude that NG can be ranked as among the most active metal-free ozonation catalysts in water. The ability of NG to act as an effective ozonation catalyst in water in the presence of common inorganic ions or organic matter (as well as when using surface river water or seawater) is also demonstrated. This is attributed to the absence of hydroxyl radical species during catalytic ozonation that could be strongly quenched by some of the inorganic ions or organic matter present in water and the formation of ROS as $^1O_2$ (as evidenced by selective quenching experiments and EPR measurements).

The authors believe that these results provide opportunities for the development of other carbon-based ozonation catalysts with applications in natural waters.

CRediT authorship contribution statement

Antón López-Francés, Investigation, Methodology. **Francisco Bernat-Quesada**, Investigation. **María Cabrero-Antonino**, Investigation. **Belén Ferrer**, Investigation. **Amarajothi Dhakshinammorthy**, Writing – review & editing. **Herme G. García,** Writing – original draft, Writing – review & editing. **Sergio Navalón,** Conceptualization, Methodology, Validation, Investigation, Resources, Writing – original draft, Writing – review & editing, Funding acquisition.

Declaration of Competing Interest

The authors declare that they have no known competing financial interests or personal relationships that could have appeared to influence the work reported in this paper.

Data Availability

Data will be made available on request.

Acknowledgements

S.N. wishes to thank the Agència Valenciana de la Innovació for its financial support (AVI, INNEST/2020/111). S.N. also thanks the support received from Grant PID2021–123856OB-I00 funded by MCIN/AEI/10.13039/501100011033 and by "ERDF A way of making Europe". S.N acknowledges the funding for open access charge from "CRUE-Universitat Politècnica de València". A.D. is beneficiary of a grant María Zambrano in Universitat Politècnica de València within the framework of the grants for the retraining in the Spanish university system (Spanish Ministry of Universities, financed by the European Union, NextGeneration EU).

Appendix A. Supporting information

Supplementary data associated with this article can be found in the online version at doi:10.1016/j.apcatb.2023.122924.

References

[1] P. Gautam, S. Kumar, S. Lokhandwala, Advanced oxidation processes for treatment of leachate from hazardous waste landfill: a critical review, J. Clean. Prod. 237 (2019), 117639, https://doi.org/10.1016/j.jclepro.2019.117639.
[2] M. Klavarioti, D. Mantzavinos, D. Kassinos, Removal of residual pharmaceuticals from aqueous systems by advanced oxidation processes, 2009, Environ. Int. (2009) 402–417, https://doi.org/10.1016/j.envint.2008.07.009.
[3] D.B. Miklos, C. Remy, M. Jekel, M. Jekel, J.E. Drewes, U. Hübner, Evaluation of advanced oxidation processes for water and wastewater treatment – a critical review, Water Res. 139 (2018) 118–131, https://doi.org/10.1016/j.watres.2018.03.042.
[4] E. Neyens, J. Baeyens, A review of classic Fenton's peroxidation as an advanced oxidation technique, J. Hazard. Mater. 98 (2003) 33–50, https://doi.org/10.1016/S0304-3894(02)00282-0.
[5] V.I. Parvulescu, F. Epron, H. Garcia, P. Granger, Recent progress and prospects in catalytic water treatment, Chem. Rev. 122 (2022) 2981–3121, https://doi.org/10.1021/acs.chemrev.1c00527.
[6] M. Pera-Titus, V. García-Molina, M.A. Baños, J. Giménez, S. Esplugas, Degradation of chlorophenols by means of advanced oxidation processes: a general review, Appl. Catal., B 47 (2004) 219–256, https://doi.org/10.1016/j.apcatb.2003.09.010.
[7] J.J. Pignatello, E. Oliveros, A. MacKay, Advanced oxidation processes for organic contaminant destruction based on the fenton reaction and related chemistry, Crit. Rev. Env. Sci. Tec. 36 (2006) 1–84, https://doi.org/10.1080/10643380500326564.
[8] M. Priyadarshini, I. Das, M.M. Ghangrekar, L. Blaney, Advanced oxidation processes: performance, advantages, and scale-up of emerging technologies, J. Environ. Manag. 316 (2022), 115295, https://doi.org/10.1016/j.jenvman.2022.115295.
[9] Y. Shang, X. Xu, B. Gao, S. Wang, X. Duan, Single-atom catalysis in advanced oxidation processes for environmental remediation, Chem. Soc. Rev. 50 (2021) 5281–5322, https://doi.org/10.1039/D0CS01032D.
[10] P. Hu, M. Long, Cobalt-catalyzed sulfate radical-based advanced oxidation: a review on heterogeneous catalysts and applications, Appl. Catal., B 181 (2016) 103–117, https://doi.org/10.1016/j.apcatb.2015.07.024.
[11] B. Kasprzyk-Hordern, M. Ziółek, J. Nawrocki, Catalytic ozonation and methods of enhancing molecular ozone reactions in water treatment, Appl. Catal. B Environ. (2003) 639–669, https://doi.org/10.1016/S0926-3373(03)00326-6.
[12] J. Nawrocki, B. Kasprzyk-Hordern, The efficiency and mechanisms of catalytic ozonation, Appl. Catal., B 99 (2010) 27–42, https://doi.org/10.1016/j.apcatb.2010.06.033.
[13] C.V. Rekhate, J.K. Srivastava, Recent advances in ozone-based advanced oxidation processes for treatment of wastewater- A review, Chem. Eng. J. Adv. 3 (2020), 100031, https://doi.org/10.1016/j.ceja.2020.100031.
[14] A. Dhakshinamoorthy, S. Navalon, M. Alvaro, H. Garcia, Metal nanoparticles as heterogeneous fenton catalyst, ChemSusChem 5 (2012) 46–64, https://doi.org/10.1002/cssc.201100517.
[15] S. Navalon, A. Dhakshinamoorthy, M. Alvaro, H. Garcia, Heterogeneous Fenton catalysts based on activated carbon and related materials, ChemSusChem 4 (2011) 1712–1730, https://doi.org/10.1002/cssc.201100216.
[16] M. Kohantorabi, G. Moussavi, S. Giannakis, A review of the innovations in metal- and carbon-based catalysts explored for heterogeneous peroxymonosulfate (PMS) activation, with focus on radical vs. non-radical degradation pathways of organic contaminants, Chem. Eng. J. 411 (2021), 127957, https://doi.org/10.1016/j.cej.2020.127957.
[17] W.-D. Oh, Z. Dong, T.-T. Lim, Generation of sulfate radical through heterogeneous catalysis for organic contaminants removal: current development, challenges and prospects, Appl. Catal., B 194 (2016) 169–201, https://doi.org/10.1016/j.cej.2020.127957.
[18] N. Chen, D. Lee, H. Kang, D. Cha, J. Lee, C. Lee, Catalytic persulfate activation for oxidation of organic pollutants: a critical review of mechanisms and controversies, J. Environ. Chem. Eng. 10 (2022), 107654, https://doi.org/10.1016/j.jece.2022.107654.
[19] X.-w Ao, J. Eloranta, C.-H. Huan, D. Santoro, W.-j Sun, Z.-D. Lu, C. Li, Peracetic acid-based advanced oxidation processes for decontamination and disinfection of water: a review, Water Res. 188 (2021), 116479, https://doi.org/10.1016/j.watres.2020.116479.
[20] T.T. Dang, V.M. Do, V.T. Trinh, Nano-catalysts in ozone-based advanced oxidation processes for wastewater treatment, Curr. Pollut. Rep. 6 (2020) 217–229, https://doi.org/10.1007/s40726-020-00147-3.
[21] S.P. Ghuge, A.K. Saroha, Catalytic ozonation for the treatment of synthetic and industrial effluents - application of mesoporous materials: a review, J. Environ. Manag. 211 (2018) 83–102, https://doi.org/10.1016/j.jenvman.2018.01.052.
[22] Z. Song, J. Sun, Z. Wang, J. Ma, Y. Liu, F.J. Javier Rivas, F.J. Juan Beltrán, W. Chu, D. Robert, Z. Chen, B. Xu, F. Qi, J. Kumirsk, E.M. Siedleck, A. Ikhlaq, Two-dimensional layered carbon-based catalytic ozonation for water purification: rational design of catalysts and an in-depth understanding of the interfacial reaction mechanism, Sci. Total Environ. 832 (2022), 155071, https://doi.org/10.1016/j.scitotenv.2022.155071.
[23] B. Wang, H. Zhang, F. Wang, X. X.;, K. Tian, Y. Sun, T. Yu, Application of heterogeneous catalytic ozonation for refractory organics in wastewater, Catalysts 9 (2019) 241, https://doi.org/10.3390/catal9030241.
[24] J. Wang, Z. Bai, Fe-based catalysts for heterogeneous catalytic ozonation of emerging contaminants in water and wastewater, Chem. Eng. J. 312 (2017) 79–98, https://doi.org/10.1016/j.cej.2016.11.118.
[25] Y. Wang, G. Yu, Challenges and pitfalls in the investigation of the catalytic ozonation mechanism: a critical review, J. Hazard. Mater. 436 (2022), 129157, https://doi.org/10.1016/j.jhazmat.2022.129157.
[26] Y. Liu, C. Chen, X. Duan, S. Wang, Y. Wang, Carbocatalytic ozonation toward advanced water purification, J. Mater. Chem. A 9 (2021) 18994–19024, https://doi.org/10.1039/D1TA02953C.
[27] U.Von Gunten, Ozonation of drinking water: Part I. Oxidation kinetics and product formation, Water Res. 37 (2003) 1443–1467, https://doi.org/10.1016/S0043-1354(02)00457-8.
[28] U.Von Gunten, Ozonation of drinking water: Part II. Disinfection and by-product formation in presence of bromide, iodide or chlorine, Water Res. 37 (2003) 1469–1487, https://doi.org/10.1016/S0043-1354(02)00458-X.
[29] D.S. Pines, D.A. Reckhow, Effect of dissolved cobalt(II) on the ozonation of oxalic acid, Environ. Sci. Technol. 36 (2002) 4046–4051, https://doi.org/10.1021/es011230w.
[30] F.J. Beltran, F.J. Rivas, R. Montero-de-Espinosa, Ozone-enhanced oxidation of oxalic acid in water with cobalt catalysts. 1.Homogeneous catalytic ozonation, Ind. Eng. Chem. Res 42 (2003) 3210–3217, https://doi.org/10.1021/ie0209982.
[31] W. Yang, T. Wu, Investigation of matrix effects in laboratory studies of catalytic ozonation processes, Ind. Eng. Chem. Res. 58 (2019) 3468–3477, https://doi.org/10.1021/acs.iecr.8b05465.
[32] X. Duan, H. Sun, S. Wang, Metal-free carbocatalysis in advanced oxidation reactions, Acc. Chem. Res. 51 (2018) 678–687, https://doi.org/10.1021/acs.accounts.7b00535.
[33] W. Huang, S. Xiao, H. Zhong, M. Yan, X. Yang, Activation of persulfates by carbonaceous materials: a review, Chem. Eng. J. 418 (2021), 129297, https://doi.org/10.1016/j.cej.2021.129297.
[34] H. Luo, H. Fu, H. Yin, Q. Lin, Carbon materials in persulfate-based advanced oxidation processes: the roles and construction of active sites, J. Hazard. Mater. (2022), 128044, https://doi.org/10.1016/j.cej.2021.129297.
[35] S. Navalon, M. Alvaro, H. Garcia, Heterogeneous Fenton catalysts based on clays, silicas and zeolites, Appl. Catal. B-Environ. 99 (2010) 1–26, https://doi.org/10.1016/j.apcatb.2010.07.006.
[36] J. Yu, L. Tang, Y. Pang, X. Liang, Y. Lu, H. Feng, J. Wang, L. Deng, J. Zou, Z. Zhu, J. Tang, Non-radical oxidation in environmental catalysis: recognition, identification, and perspectives, Chem. Eng. J. 433 (2022), 134385, https://doi.org/10.1016/j.cej.2021.134385.
[37] P.M. Alvárez, F.J. Beltrán, F.J. Masa, J.P. Pocostales, A comparison between catalytic ozonation and activated carbon adsorption/ozone-regeneration processes for wastewater treatment. Appl. Catal., B 92 (2009) 393–400, https://doi.org/10.1016/j.cej.2021.134385.
[38] P.M. Alvarez, J.F. García-Araya, F.J. Beltrán, I. Giráldez, J. Jaramillo, V. Gomez-Serrano, The influence of various factors on aqueous ozone decomposition by granular activated carbons and the development of a mechanistic approach, Carbon 44 (2006) 3102–3112, https://doi.org/10.1016/j.carbon.2006.03.016.
[39] P.C.C. Faria, J.J.M. Orfao, M.F.R. Pereira, Catalytic ozonation of sulfonated aromatic compounds in the presence of activated carbon, Appl. Catal., B 83 (2008) 150–159, https://doi.org/10.1016/j.apcatb.2008.02.010.

[40] P.C.C. Faria, J.J.M. Órfão, M.F.R. Pereira, Ozone decomposition in water catalysed by activated carbon: influence of chemical and textural properties, Ind. Eng. Chem. Res. 45 (2006) 2715–2721, https://doi.org/10.1021/ie060056n.
[41] A.G. Gonçalves, J.J.M. Órfão, M.F.R. Pereira, Catalytic ozonation of sulphamethoxazole in the presence of carbon materials, J. Hazard. Mater. 239−240 (2012) 167–174, https://doi.org/10.1016/j.jhazmat.2012.08.057.
[42] M. Sánchez-Polo, U. von Gunten, J. Rivera-Utrilla, Efficiency of activated carbon to transform ozone into OH radicals: Influence of operational parameters, Water Res 39 (2005) 3189–3198, https://doi.org/10.1016/j.watres.2005.05.026.
[43] O.S.G.P. Soares, P.C.C. Faria, J.J.M. Órfão, M.F.R. Pereira, Ozonation of textile effluents and dye solutions in the presence of activated carbon under continuous operation, Sep. Sci. Technol. 2007 42 (2007) 1477–1492, https://doi.org/10.1080/01496390701290102.
[44] A.G. Gonçalves, J.L. Figueiredo, J.J.M. Orfao, M.F.R. Pereira, Influence of the surface chemistry of multi-walled carbon nanotubes on their activity as ozonation catalysts, Carbon 48 (2010) 4369–4381, https://doi.org/10.1016/j.carbon.2010.07.051.
[45] J. Restivo, C.A. Alexandra Orge, A.S. Guedes Gorito dos Santos, O.S.G. Pinto Soares, M.F. Ribeiro Pereira, Nanostructured layers of mechanically processed multiwalled carbon nanotubes for catalytic ozonation of organic pollutants, ACS Appl. Nano Mater. 3 (2020) 5271–5284, https://doi.org/10.1021/acsanm.0c00662.
[46] J. Wang, S. Chen, X. Quan, H. Yu, Fluorine-doped carbon nanotubes as an efficient metal-free catalyst for destruction of organic pollutants in catalytic ozonation, Chemosphere 190 (2018) 135–143, https://doi.org/10.1016/j.chemosphere.2017.09.119.
[47] Y. Wang, H. Cao, L. Chen, C. Chen, X. Duan, Y. Xie, W. Song, H. Sune, S. Wang, Tailored synthesis of active reduced graphene oxides from waste graphite: structural defects and pollutant-dependent reactive radicals in aqueous organics decontamination, Appl. Catal. B. Environ. 229 (2018) 71–80, https://doi.org/10.1016/j.apcatb.2018.02.010.
[48] F. Bernat-Quesada, J.C. Espinosa, V. Barbera, M. Álvaro, M. Galimberti, S. Navalon, H. García, Catalytic ozonation using edge-hydroxylated graphite-based materials, ACS Sustain. Chem. Eng. 7 (2019) 17443–17452, https://doi.org/10.1021/acssuschemeng.9b04646.
[49] Y. Wang, Y. Xie, H. Sun, J. Xiao, H. Cao, S. Wang, Efficient catalytic ozonation over reduced graphene oxide for p-hydroxylbenzoic acid (PHBA) destruction: active site and mechanism, ACS Appl. Mater. Interfaces 8 (2016) 9710–9720, https://doi.org/10.1021/acsami.6b01175.
[50] F. Bernat-Quesada, C. Vallés-García, E. Montero-Lanzuela, A. López-Francés, B. Ferrer, H.G.G. Baldoví, S. Navalón, Hybrid sp2/sp3 nanodiamonds as heterogeneous metal-free ozonation catalysts in water, Appl. Catal. B. Environ. 299 (2021), 120673, https://doi.org/10.1016/j.apcatb.2021.120673.
[51] J. Restivo, J.J.M. Órfão, M.F.R. Pereira, E. Vanhaecke, M. Rönning, T. Iouranova, L. Kiwi-Minsker, S. Armenise, E. Garcia-Bordeje, Catalytic ozonation of oxalic acid using carbon nanofibres on macrostructured supports, Water Sci. Technol. 65 (2012) 1854–1862, https://doi.org/10.2166/wst.2012.882.
[52] Y. Wang, L. Chen, C. Chen, J. Xi, H. Cao, X. Duan, Y. Xie, W. Song, S. Wang, Occurrence of both hydroxyl radical and surface oxidation pathways in N-doped layered nanocarbons for aqueous catalytic ozonation, Appl. Catal. B. Environ. 254 (2019) 283–291, https://doi.org/10.1016/j.apcatb.2019.05.008.
[53] Y. Wang, X. Duan, Y. Xie, H. Sun, S. Wang, Nanocarbon-based catalytic ozonation for aqueous oxidation: engineering defects for active sites and tunable reaction pathways, ACS Catal. 10 (2020) 13383–13414, https://doi.org/10.1021/acscatal.0c04232.
[54] B. Chen, F. Li, Z. Huang, G. Yuan, Recyclable and selective nitroarene hydrogenation catalysts based on carbon-coated cobalt oxide nanoparticles, ChemCatChem 8 (2016) 1132–1138, https://doi.org/10.1002/cctc.201501265.
[55] D. Li, X. Guo, H. Song, T. Sun, J. Wan, Preparation of RuO2-TiO2/Nano-graphite composite anode for electrochemical degradation of ceftriaxone sodium, J. Hazard. Mater. (2018) 250–259, https://doi.org/10.1016/j.jhazmat.2018.03.007.
[56] D.R. Chowdhury, C. Singh, A. Paul, Role of graphite precursor and sodium nitrate in graphite oxide synthesis, RSC Adv. 4 (2014) 15138–15145, https://doi.org/10.1039/C4RA01019A.
[57] D. González, M.A. Montes-Morán, I. Suárez-Ruiz, A.B. Garcia, Structural characterization of graphite materials prepared from anthracites of different characteristics: a comparative analysis, Energy Fuels 18 (2004) 365–370, https://doi.org/10.1021/ef030144.
[58] I.C. Popovici, S. Birghila, G. Voicu, V. Ionescu, V. Ciupină, G. Prodan, Morphological and microstructural characterization of some petroleum cokes as potential anode materials in lithium-ion batteries, J. Optoelectron. Adv. Mater. 9 (2010) 1903–1908.
[59] B. Daelemans, N. Bilbao, W. Dehaen, S. De Feyter, Carbocatalysis with pristine graphite: on-surface nanochemistry assists solution-based catalysis, Chem. Soc. Rev. 50 (2021) 2280–2296, https://doi.org/10.1039/D0CS01294G.
[60] A.S. Kama, R. Othman, N.H. Jabarullah, Preparation and synthesis of synthetic graphite from biomass waste: a review, Sys Rev. Pharm. 11 (2020) 881–894.
[61] P. Murugan, R.D. Nagarajan, B.H. Shetty, M. Govindasamy, A.K. Sundramoorthy, Recent trends in the applications of thermally expanded graphite for energy storage and sensors - a review, Nanoscale Adv. 3 (2021) 6294–6309, https://doi.org/10.1039/D1NA00109D.
[62] R. Lan, W. Su, J. Li, Preparation and catalytic performance of expanded graphite for oxidation of organic pollutant, Catalysts 9 (2019) 280 (Preparation and catalytic performance of expanded graphite for oxidation of organic pollutant).
[63] Y. Song, S. Feng, W. Qin, J. Ma, Mechanism of catalytic ozonation in expanded graphite aqueous suspension for the degradation of organic acids, Environ. Technol. (2021), https://doi.org/10.1080/09593330.2021.1983024.
[64] E. Díaz, S. Ordóñez, R.F. Bueres, E. Asedegbega-Nieto, H. Sastre, High-surface area graphites as supports for hydrodechlorination catalysts: Tuning support surface chemistry for an optimal performance, Appl. Catal. B. Environ. 99 (2010) 181–190, https://doi.org/10.1016/j.apcatb.2010.06.016.
[65] P. Gallezot, S. Chaumet, A. Perrard, P. Isnard, Catalytic wet air oxidation of acetic acid on carbon-supported ruthenium catalysts, J. Catal. 168 (1997) 104–109, https://doi.org/10.1006/jcat.1997.1633.
[66] M.V. Morales, J.M. Conesa, A. Guerrero-Ruiz, I. Rodríguez-Ramos, Tunable selectivity of Ni catalysts in the hydrogenation reaction of 5-hydroxymethylfurfural in aqueous media: Role of the carbon supports, Carbon 182 (2021) 265–275, https://doi.org/10.1016/j.carbon.2021.06.007.
[67] M.R. Acocella, G. Guerra, Graphene-based carbocatalysts for thermoset polymers and for diastereoselective and enantioselective organic synthesis, ChemCatChem 10 (2018) 2350–2359, https://doi.org/10.1002/cctc.201702015.
[68] D. Bogachuk, R. Tsuji, D. Martineau, S. Narbey, J.P. Herterich, L. Wagner, K. Suginuma, S. Ito, A. Hinsch, Comparison of highly conductive natural and synthetic graphites for electrodes in perovskite solar cells, Carbon 178 (2021) 10–18, https://doi.org/10.1016/j.carbon.2021.01.022.
[69] M. Galimberti, V. Barbera, S. Guerra, L. Conzatti, C. Castiglioni, L. Brambilla, A. Serafinia, Biobased Janus molecule for the facile preparation of water solutions of few layer graphene sheets, RSC Adv. 5 (2015) 81142–81152, https://doi.org/10.1039/C5RA11387C.
[70] D.B. Schuepfer, F. Badaczewski, J.M. Guerra-Castro, D.M. Hofmann, C. Heiliger, B. Smarsly, P.J. Klar, Assessing the structural properties of graphitic and nongraphitic carbons by Raman spectroscopy, Carbon 161 (2020) 359–372, https://doi.org/10.1016/j.carbon.2019.12.094.
[71] J.P. Haase, S. Kaalberg, C.T. Redmond, M.J. Nalbandian, D.M. Cwiertny, Hydroxyl radical formation during ozonation of multiwalled carbon nanotubes: performance optimization and demonstration of a reactive CNT filter, Environ. Sci. Technol. 49 (2015) 3687–3697, https://doi.org/10.1021/es505430v.
[72] M. Wang, Z. Wang, Y. Wang, R. Li, Y. Zhang, C. Liu, Y. Liu, B. Xu, F. Qi, Insights into heteroatom-doped graphene for catalytic ozonation: active centers, reactive oxygen species evolution, and catalytic mechanism, Environ. Sci. Technol. 53 (2019) 5337–5348, https://doi.org/10.1021/acs.est.9b01361.
[73] W. Yuan, Y. Zhou, Y. Li, C. Li, H. Peng, J. Zhang, Z. Liu, L. Dai, G. Shi, The edge- and basal-plane-specific electrochemistry of a single-layer graphene sheet, Sci. Rep. 3 (2013) 2248, https://doi.org/10.1038/srep02248.
[74] J.L. Figueiredo, M.F.R. Pereira, M.M.A. Freitas, J.J.M. Orfao, Modification of the surface chemistry of activated carbons, Carbon 37 (1999) 1379–1389, https://doi.org/10.1016/S0008-6223(98)00333-9.
[75] J.C. Espinosa, Manickam-Periyaraman, Bernat-Quesada, Sivanesan, lvaro, García, S. Navalón, Engineering of activated carbon surface to enhance the catalytic activity of supported cobalt oxide nanoparticles in peroxymonosulfate activation, Appl. Catal. B. Environ. 249 (2019) 42–53, https://doi.org/10.1016/j.apcatb.2019.02.043.
[76] J. Wang, H. Chen, Catalytic ozonation for water and wastewater treatment: recent advances and perspective, Sci. Total Environ. 704 (2020), 135249, https://doi.org/10.1016/j.scitotenv.2019.135249.
[77] X. Duan, Z. Ao, H. Zhang, M. Saunders, H. Sun, Z. Shao, S. Wang, Nanodiamonds in sp2/sp3 configuration for radical to nonradical oxidation: core-shell layer dependence, Appl. Catal. B. Environ. 222 (2018) 176–181, https://doi.org/10.1016/j.apcatb.2017.10.007.
[78] Y. Wang, J. Xi, X. Duan, W. Lv, H. Cao, C. Chen, Z. Guo, Y. Xie, S. Wang, The duet of surface and radical-based carbocatalysis for oxidative destructions of aqueous contaminants over built-in nanotubes of graphite, J. Hazard. Mater. 384 (2020), 121486, https://doi.org/10.1016/j.jhazmat.2019.121486.
[79] A.I. Martiryan, T.M. Ayvazyan, S.A. Markarian, Determination of the reaction rate constant for the interaction of diethyl sulfoxide with the hydroxyl radical on the basis of competitive kinetics, Proc. YSU B: Chem. Biol. Sci. 52 (2018) 80–82, https://doi.org/10.46991/PYSU:B/2018.52.2.080.
[80] J. Staehelin, J. Hoigne, Decomposition of ozone in water in the presence of organic solutes acting as promoters and inhibitors of radical chain reactions, Environ. Sci. Technol. 19 (1985) 1206–1213, https://doi.org/10.1021/es00142a012.
[81] J.J. Wu, M. Muruganandham, S.H. Chen, Degradation of DMSO by ozone-based advanced oxidation processes, J. Hazard. Mater. 149 (2007) 218–225, https://doi.org/10.1016/j.jhazmat.2007.03.071.
[82] O. Fónagy, E. Szabó-Bárdos, O. Horváth, 1,4-benzoquinone and 1,4-hydroquinone based determination of electron and superoxide radical formed in heterogeneous photocatalytic system, J. Photochem. Photobiol. A. 407 (2021), 113057, https://doi.org/10.1016/j.jphotochem.2020.113057.
[83] H.A. Aboubakr, U. Gangal, M.M. Youssef, S.M. Goyal, P.J. Bruggeman, Inactivation of virus in solution by cold atmospheric pressure plasma: identification of chemical inactivation pathways, J. Phys. D: Appl. Phys. 49 (2016), 204001, https://doi.org/10.1088/0022-3727/49/20/204001.
[84] E. Appiani, R. Ossola, D.E. Latch, P.R. Erickson, K. McNeill, Aqueous singlet oxygen reaction kinetics of furfuryl alcohol: effect of temperature, pH, and salt content, Environ. Sci.: Process. Impacts 19 (2017) 507–516.
[85] Z. Barbieriková, M. Mihalíková, V. Brezová, Photoinduced oxidation of sterically hindered amines in acetonitrile solutions and titania suspensions (an EPRstudy), Photochem. Photobio. 88 (2012) 1442–1454, https://doi.org/10.1111/j.1751-1097.2012.01189.x.

[86] P. Bilski, K. Reszka, M. Bilska, C.F. Chignell, Oxidation of the spin trap 5,5-dimethyl-1-pyrroline n-oxide by singlet oxygen in aqueous solution, J. Am. Chem. Soc. 118 (1996) 1330–1338, https://doi.org/10.1021/ja952140s.
[87] J. Marcon, G. Mortha, N. Marlin, F. Molton, C. Duboc, A. Burnet, New insights into the decomposition mechanism of chlorine dioxide at alkaline pH, Holzforschung 71 (2017) 599–610, https://doi.org/10.1515/hf-2016-0147.
[88] S.R. Plimpton, M. Gołkowski, D.G. Mitchell, C. Austin, S.S. Eaton, G.R. Eaton, C. G. Gołkowski, M. Voskuil, Remote delivery of hydroxyl radicals via secondary chemistry of a nonthermal plasma effluent, Biotech. Bioeng. 110 (2013) 1936–1944, https://doi.org/10.1002/bit.24853.
[89] S. Sharma, A. Sharma, Recent advances in photocatalytic manipulations of Rose Bengal in organic synthesis, Org. Biomol. Chem. 17 (2019) 4384–4405, https://doi.org/10.1039/C9OB00092E.
[90] Y. Yuan, M. Mortazavi, S. Garg, J. Ma, T.D. Wait, Comparison of performance of conventional ozonation and heterogeneous catalytic ozonation processes in phosphate- and bicarbonate-buffered solutions, ACS EST Engg 2 (2022) 210–221, https://doi.org/10.1021/acsestengg.1c00350.
[91] I.C. Guzmán, J.L. Rodríguez S, T. Poznyak, I. Chairez, Effect of sulphate and chloride ions on the oxidation of phenolic compounds by ozonation catalyzed with CeO2, Ozone.: Sci. Eng. 43 (2021) 592–605, https://doi.org/10.1080/01919512.2021.1892475.
[92] M. Li, K. Yang, X. Huang, S. Liu, Y. Jia, P. Gu, H. Miao, Efficient degradation of trimethoprim by catalytic ozonation coupled with Mn/FeOx-functionalized ceramic membrane: synergic catalytic effect and enhanced anti-fouling performance, J. Coll. Interf. Sci. 616 (2022), https://doi.org/10.1016/j.jcis.2022.02.061.
[93] H. Miao, W.Wenyi Tao, Ozonation of humic acid in water, Chem. Technol. Biotechnol. 83 (2008) 336–344, https://doi.org/10.1002/jctb.1816.